8-1988

Recoil Corrected Continuum Shell Model Form Factor Calculations For $^{4}He(e,e')^{4}He(0+)$

Jiang Yu

RECOIL CORRECTED CONTINUUM SHELL MODEL FORM FACTOR CALCULATIONS FOR ^{4}He(e, e')^{4}He(0^+)

by

Jiang Yu

A Thesis
Submitted to the
Faculty of The Graduate College
in partial fulfillment of the
requirements for the
Degree of Master of Arts
Department of Physics

Western Michigan University
Kalamazoo, Michigan
August 1988

RECOIL CORRECTED CONTINUUM SHELL MODEL FORM FACTOR CALCULATIONS FOR $^4He(e,e')^4He(0^+)$

Jiang Yu, M. A.

Western Michigan University, 1988

Charge form factor calculations for the electroexcitation of the ^4He, 0^+ state have been performed within the context of the recoil corrected continuum shell model. A pure $0s^4$ ground state structure is assumed and full internal coordinate recoil corrections are made. The result is compared with available data. It is demonstrated that the 0^+ state may be described in a 1p-1h shell model context. Inclusion of $ns0s^{-1}$ ground state correlations is suggested for further reseach.

ACKNOWLEDGEMENTS

I would like to express my infinite gratitude to Professor Dean Halderson for all of his guidance and patience throughout this research. It is also with pleasure that I would like to thank Professor Alvin Rosenthal and Professor Michitoshi Soga for taking the time to serve on my committee.

Jiang Yu

INFORMATION TO USERS

This reproduction was made from a copy of a document sent to us for microfilming. While the most advanced technology has been used to photograph and reproduce this document, the quality of the reproduction is heavily dependent upon the quality of the material submitted.

The following explanation of techniques is provided to help clarify markings or notations which may appear on this reproduction.

1. The sign or "target" for pages apparently lacking from the document photographed is "Missing Page(s)". If it was possible to obtain the missing page(s) or section, they are spliced into the film along with adjacent pages. This may have necessitated cutting through an image and duplicating adjacent pages to assure complete continuity.

2. When an image on the film is obliterated with a round black mark, it is an indication of either blurred copy because of movement during exposure, duplicate copy, or copyrighted materials that should not have been filmed. For blurred pages, a good image of the page can be found in the adjacent frame. If copyrighted materials were deleted, a target note will appear listing the pages in the adjacent frame.

3. When a map, drawing or chart, etc., is part of the material being photographed, a definite method of "sectioning" the material has been followed. It is customary to begin filming at the upper left hand corner of a large sheet and to continue from left to right in equal sections with small overlaps. If necessary, sectioning is continued again—beginning below the first row and continuing on until complete.

4. For illustrations that cannot be satisfactorily reproduced by xerographic means, photographic prints can be purchased at additional cost and inserted into your xerographic copy. These prints are available upon request from the Dissertations Customer Services Department.

5. Some pages in any document may have indistinct print. In all cases the best available copy has been filmed.

University Microfilms International
300 N. Zeeb Road
Ann Arbor, MI 48106

Order Number 1334644

Recoil corrected continuum shell model form factor calculations for $^4He(e, e')^4He(0^+)$

Yu, Jiang, M.A.

Western Michigan University, 1988

U·M·I
300 N. Zeeb Rd.
Ann Arbor, MI 48106

TABLE OF CONTENTS

ACKNOWLEDGEMENTS ii

LIST OF TABLES iv

LIST OF FIGURES v

CHAPTER

I. INTRODUCTION 1

Electron Scattering 1

The Recoil Corrected Continuum Shell Model 6

The First Excited State of ^{4}He Structure Investigation 10

II. DERIVATION OF CHARGE FORM FACTORS FOR ^{4}He 15

III. THE CALCULATION AND THE RESULTS 27

IV. CONCLUSION AND A SUGGESTION FOR FURTHER RESEARCH 35

APPENDICES

A. Experimental Data From Kobschall et al., 1983 37

B. Experimental Data From Walcher, 1970 39

C. Experimental Data From Frosch et al., 1965 41

BIBLIOGRAPHY 43

LIST OF TABLES

1. Differential Cross Section of Quasi-Bound State of ^{4}He. (From Kobschall et al., 1983) 38

2. Experimental Results for the 20.5 MeV Level of the α Particle. (From Walcher, 1970) 40

3. Experimental Results for the 20 MeV Level of the α Particle. (From Frosch et al., 1965) 42

LIST OF FIGURES

1. A Typical Double Differential Electron Scattering Cross Section 3
2. The General Electron Scattering Process in Lowest Order in α 4
3. Observed and RCCSM Calculated Positions of Bound States and Resonances Below E_p(c.m.) = 10 MeV 10
4. Experimental Double Differential Cross Section of The Break-up continuum at an Incident Energy E_o = 320 MeV and a Scattering Angle $\theta = 44.96^o$ 11
5. Internal Coordinates Within ^{4}He System 13
6. Coordinate Transformation Within ^{4}He System 17
7. Spin Coupling for The Core of ^{4}He(0^+) 19
8. ME(1) vs. q for n = 1, 2, 3, 4, 5, 6, 7 29
9. 0.5 ME(3) vs. q for n = 1, 2 29
10. 0.5 ME(3) vs. q for n = 2, 3, 4 30
11. 0.5 ME(3) vs. q for n = 4, 5, 6 30
12. The Calculated RCCSM F(q, E_p) 32
13. The Calculated RCCSM Charge Form Factors F(q^2) 33
14. Cross Section for the ^{4}He(γ , p)^{3}H reaction 36

CHAPTER I

INTRODUCTION

Electron Scattering

Two fundamental reasons have made electron scattering an important and powerful tool in studying nuclear structure. For the first, in contrast to the situation with strongly interacting projectiles, where the scattering mechanism cannot be clearly separated from structure effects in the target, the interaction between the electron and the target nucleons in electron scattering is completely known. Also, the electron interaction with the electromagnetic charge and current density of the nucleus is relatively weak, of order $\alpha = 1/137$, so that one can immediately relate the cross section to the transition matrix elements of the local charge and current density operators and thus directly to the structure of the target itself. Though the same considerations also apply to processes involving real photons, the second reason offers electrons the other great advantage which real photons do not have. That is, for a fixed energy loss w of the electron, one can vary the three-momentum transferred to the nucleus, **q**, with the only restriction that the four momentum transfer be space-like, i.e.,

$$q_\mu^2 = q^2 - w^2 > 0 \qquad (1.1)$$

for electrons. For a given energy transfer in the case of real

photons, there is only a single possible momentum transfer,

$$q_\mu^2 = q^2 - w^2 = 0, \tag{1.2}$$

since the mass of a real photon is zero. Thus with electrons, one can study the complete q^2 behavior of the transition matrix elements and map out the Fourier transforms of the transition charge and current densities. Therefore, one knows the spatial distribution of the transition change and current densities themselves, and this is certainly a source of tremendously rich and unique information on the structure of nuclei.

Five regions can be identified in the electron scattering spectrum illustrated in figure 1 (DeForest & Walecka, 1966). Here the ordinate stands for double differential cross section of electron scattering, which is a function of the other two variables, w the energy loss,

$$w = E_1 - E_2, \tag{1.3}$$

and q the three-momentum transfer,

$$q^2 = q^2 . \tag{1.4}$$

Figure 1 is really a "theorist's" spectrum for a fixed θ, the scattering angle.

The first region is related to elastic scattering, the situation where (except for nuclear recoil) $w = 0$. The electrons are scattered from the nucleus, leaving the nucleus in its ground state. Many experiments on elastic scattering have been carried out, and the best information so far on nuclear size comes from elastic electron scattering. The next region of the spectrum, $w > 0$, corresponds to inelastic scattering. One can see spikes

coresponding to the excitation of nuclear levels. In this region, since w > 0, the electrons leave the nucleus with lower energy than that of the incident electrons, leading the nucleus to its excited states. Therefore the electro-excitation provides a fairly sensitive test for theories which attempt to describe such levels and can also help to give other nuclear structure information.

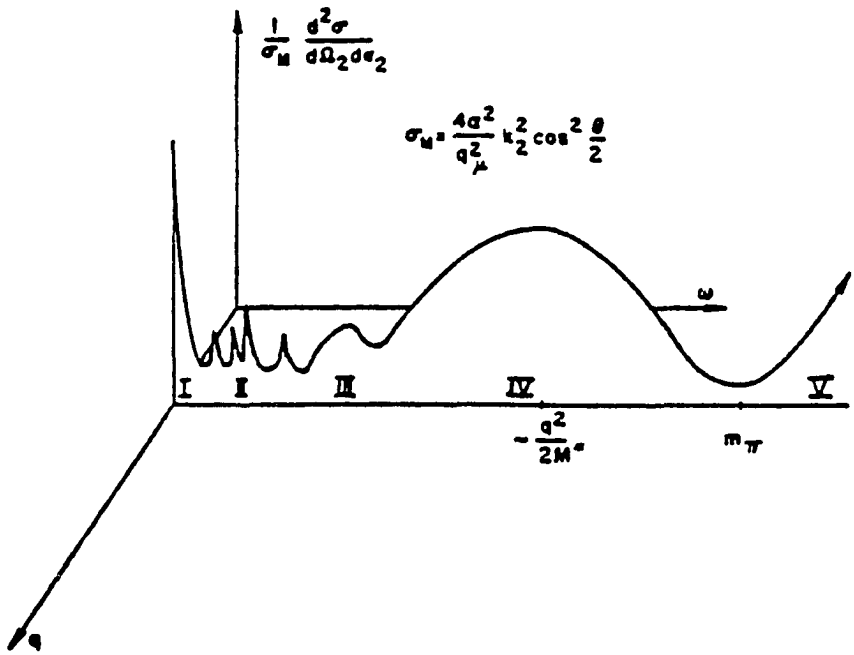

Figure 1. A Typical Double Differential Electron Scattering Cross Section.

The third region is giant resonance region characterized by collective motion. The fourth region of the spectrum is a broad peak which is referred to as the quasi-elastic peak. It corresponds to direct collisions with the individual nucleons in the nucleus and occurs at $w = q^2/2M^*$, with the total width given roughly by

$$q\cdot k_F/M^* + q^2/2M^* \geq W \geq -q\cdot k_F/M^* + q^2/2M^*.$$

Here, M^* is an effective mass for the nucleon and takes the

binding energy into account, and k_F is the Fermi momentum ($k_F \sim 250$ MeV). One can hopefully obtain information about two-particle correlations from this region. Last, the fifth region belongs to meson production, which starts at $w = m_\pi$. Meson production gives different information on nuclear structure and nucleon structure.

Figure 2 indicates the general electron scattering process through a single photon exchange. The initial and final four-momenta of the target are P_μ and P'_μ and of the electron are $k_{1\mu}$ and $k_{2\mu}$.

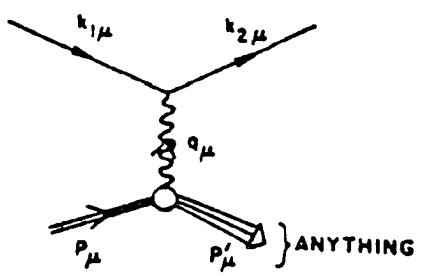

Figure 2. The General Electron Scattering Process in Lowest Order in α .

For the process, the double differential cross section in the laboratory frame (neglecting the mass of the electron) can be written as (DeForest & Walecka, 1966):

$$(d^2\sigma/d\Omega_2 dE_2) = (4Z^2\alpha^2/q_\mu^4)(E_2^2/M_T)\{\cos^2(\theta/2)\cdot[W_2(q_\mu^2, q\cdot P) + 2W_1(q_\mu^2, q\cdot P)\cdot\tan^2(\theta/2)]\}. \quad (1.5)$$

$$q_\mu^2 = 4E_1E_2\sin^2(\theta/2) . \quad (1.6)$$

$$M_T^2 = -P_\mu^2 . \quad (1.7)$$

where $W_{1,2}(q_\mu^2, q\cdot P)$ are two form factors and can be separated experimentally by doing experiments at fixed q_μ^2 and $q\cdot P$, then

varying the angle θ.

$W_{1,2}(q_\mu^2, q\cdot P)$ can be related to the structure of the nucleus. Briefly, one writes the interaction of the electron with the nucleus as

$$\hat{H}_1(x) = - e\hat{j}_\mu(x)A_\mu^{ext}(x), \tag{1.8}$$

where

$$\hat{j}_\mu(x) = i\psi(x)\gamma_\mu\psi(x) \tag{1.9}$$

for the point-like electron. The external potential is due to the nucleus and is related to the nuclear current by

$$\Box A_\mu^{ext}(x) = - e_p J_\mu(x) = - e_p \langle f| \hat{J}_\mu(x) | i\rangle. \tag{1.10}$$

Matrix elements of the interaction, $\hat{H}_1(x)$, can be put in terms of the nuclear current by the Fourier transform

$$q_\mu^2 \int \exp\{-iq.x\}.A_\mu^{ext}(x)d^4x = e_p \int \exp\{-iq.x\}.J_\mu(x)d^4x = e_p J_\mu(q).$$

The customary multipole expansion of the nuclear current $J_\mu(q)$ leads to

$$\begin{aligned}(d\sigma/d\Omega) = \{ & (8\pi\alpha^2 E_2/q_\mu^4 \cdot E_1)/[1 + (E_2 - E_1\cos\theta)/E'] \ \} \\ & \cdot \{ \ V_L(\theta)\sum_{J=0}^{\infty}[\ |\langle J_f \| \hat{M}_J^{coul}(q) \| J_i\rangle|^2/(2J_i + 1)] \\ & + V_T(\theta)\sum_{J=1}^{\infty}[(|\langle J_f \| \hat{T}_J^{el}(q) \| J_i\rangle|^2/(2J_i + 1)) \\ & + (|\langle J_f \| \hat{T}_J^{mag}(q) \| J_i\rangle|^2/(2J_i + 1))] \ \} ,\end{aligned} \tag{1.11}$$

where

$$V_L(\theta) = 2(q_\mu^4/q^4)E_1E_2\cdot\cos^2(\theta/2), \tag{1.12}$$

$$V_T(\theta) = (2E_1E_2/q^2)\cdot\sin^2(\theta/2)\cdot[\ (E_1+E_2)^2 - 2E_1E_2\cdot\cos^2(\theta/2) \ ]. \tag{1.13}$$

Therefore the electron scattering problem reduces to calculation of conventional multipole operators between initial and final nuclear

states.

Inelastic electron scattering is considered very important and useful in nuclear structure studies, especially on the structure of nuclear excitations. Since the nucleus is led to its higher energy levels while electrons are scattered from it with energy loss, W > 0, the cross section can give information on form factors and therefore the structure of the excited states. Also, one can theoretically predict the energy levels of a nucleus and the form factors by using nuclear structure models, and then compare the theoretical results with experimental data for the same system in order to examine whether the models adequately describe that system.

The Recoil Corrected Continuum Shell Model

Since a detailed knowledge of nuclear forces within a nucleus as a many-body system is unknown, the method of nuclear models has been used to investigate the structure of nuclei. This method consists of constructing a physical system, the model, with which we can perform calculations and whose properties resemble a nucleus. The physics of the model are studied and it is hoped that any properties thus discovered will also be properties of the nucleus. Then the structure of the model will stand for the structure of the nucleus. No single model can account for all the known facts about nuclei. So far, several models have successfully approached different aspects of the physics of nuclei. One of the models is the shell model, which has explained

not only the main features of the shell structure phenomena, but also more detailed properties such as the spins, magnetic moments, and level spectra of many nuclei.

The shell model is based on the experimental evidence that some certain numbers of neutrons or protons such as,

2, 8, 20, 28, 50, 82, 126,

lead to particular stability of nuclei (for examples of the experiments, see the article by Flowers in 1952). These numbers are called magic numbers, and the phenomena have been interpreted as an indication that neutrons and protons within the nucleus are arranged into shells within the nucleus, like electrons in atoms. Each shell is limited to a certain maximum number of nucleon of a given sort. When a shell is filled, the resulting configuration is particularly stable and therefore of low energy. The shell model is built up under the following two assumptions:

1. The "central" potential is really an average potential, and the addition of an extra nucleon modifies this potential far more than the addition of an extra electron modifies the central potential in the atomic case.

2. Because of the Coulomb repulsion of the protons, the numbers of neutrons and protons in a nucleus are not even approximately the same in all but the lightest nuclides. It is therefore most unlikely that a nuclide with a closed shell number of neutrons can also have a closed shell number of protons and conversely. The stability characteristics of closed shells will therefore be less marked than in the atomic case.

For general consideration, a non-relativistic system of A nucleons is characterized by a Hamiltonian H = H (1, ..., A). The numbers 1, ··· , A stand for the space, spin and isospin coordinates of the A nucleons. H can be decomposed into two parts,

$$H = H_0 + B, \tag{1.14}$$

where H_0 is a shell-model Hamiltonian, a sum of single particle operators

$$H_0 = \sum_{i=1}^{A} h_0(i) = \sum_{i=1}^{A} [t(i) + v_0(i)] . \tag{1.15}$$

Here t(i) is the kinetic energy operator, while $v_0(i)$ is the shell model potential. The residual interaction B is a sum over one- and two-body potentials. To describe a scattering problem, $v_0(i)$ must be a potential of finite depth. In the usual bound-state calculations, $v_0(i)$ is chosen to be a potential of infinite depth, usually a harmonic oscillator potential.

In the conventional shell model, the basic ansatz is an expansion of the wave function in terms of products of single-particle functions. This ansatz is very flexible and is also very convenient for such operations as the calculation of matrix elements and the proper treatment of the Pauli principle. But because of the presence of unbound states, the conventional shell model cannot be applied to the nuclear reactions involving one particle in the continuum. The separability of the c.m. coordinate can be conveniently imposed in the model only if harmonic oscillator expansion functions are employed, but this leads to an infinite number of discrete bound states, and no continuous set of eigenstates. To solve this problem, Fano (1961) introduced

originally and many researchers developed the continuum shell model. One continuum shell model employs R-matrix techniques (Lane & Tomas, 1958; Land & Robson, 1966, 1969; Philpott & George, 1974) so that the physical content of the model, for which the interaction region is of relatively small extent, can be expressed within a finite basis of oscillator functions. This enables the c.m. coordinate to be completely eliminated from the problems.

The continuum shell model has been applied to a wide variety of nuclear problems including all those involving a particle in the continuum. However, when the conventional continuum shell model is applied to light nuclei, the calculations contain errors of unknown magnitude which are attributable to unphysical excitation of the c. m. coordinate. Philpott then introduced the recoil corrected continuum shell model (RCCSM) in 1977, with an application to elastic scattering of a nucleon from a closed-shell target nucleus. In the RCCSM, the effects of the target nucleus recoil are considered. In 1979 Halderson and Philpott (Halderson & Philpott, 1979) extended the RCCSM to the 1p-1h states of light systems of four nucleons, and excellent agreement was obtained between the calculated and observed cross sections and polarization variables. Figure 3 shows the observed (Fiarman & Meyerhoff, 1973) and calculated positions of bound states and resonances below E_p(c.m.) = 10 MeV with and without the recoil correction.

The RCCSM calculation reproduce the first three excited

states very well. The importance of the c.m. corrections was made amply evident by a comparison with the corresponding uncorrected results.

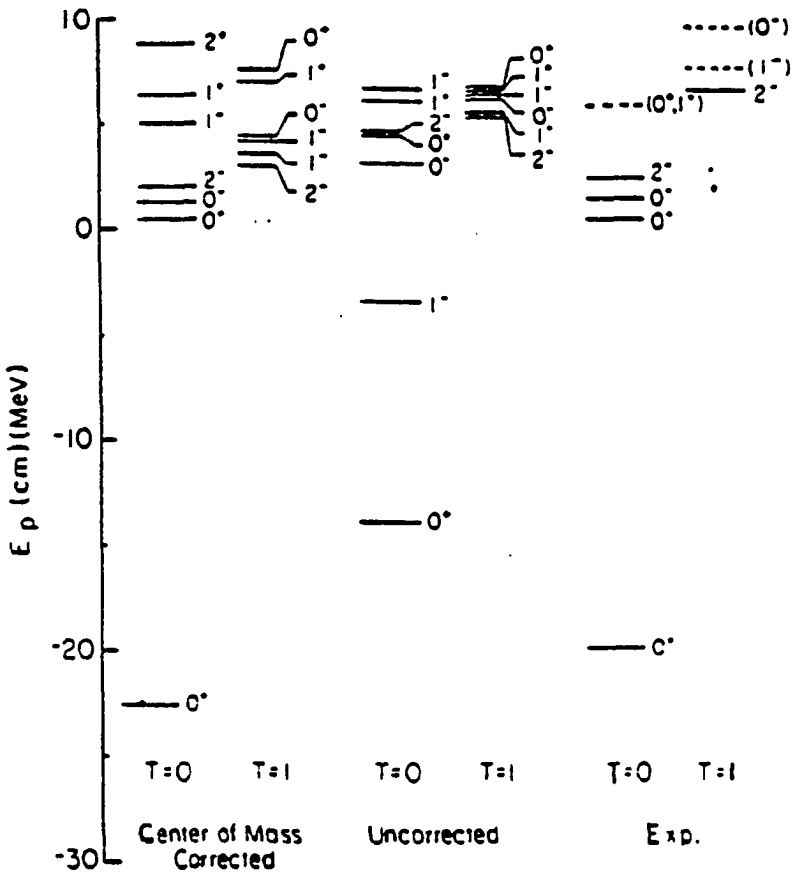

Figure 3. Observed and RCCSM Calculated Positions of Bound States and Resonances Below E_p(c.m.) = 10 MeV.

The First Excited State of ^{4}He Structure Investigation

The first excited state of ^{4}He is a 0^+ state or the breathing mode of the nucleus. Figure 4 shows (a) the double-differential cross section of the break-up continuum with its peak at an incident energy E_0 = 320 Mev and a scattering angle θ = 44.96°;

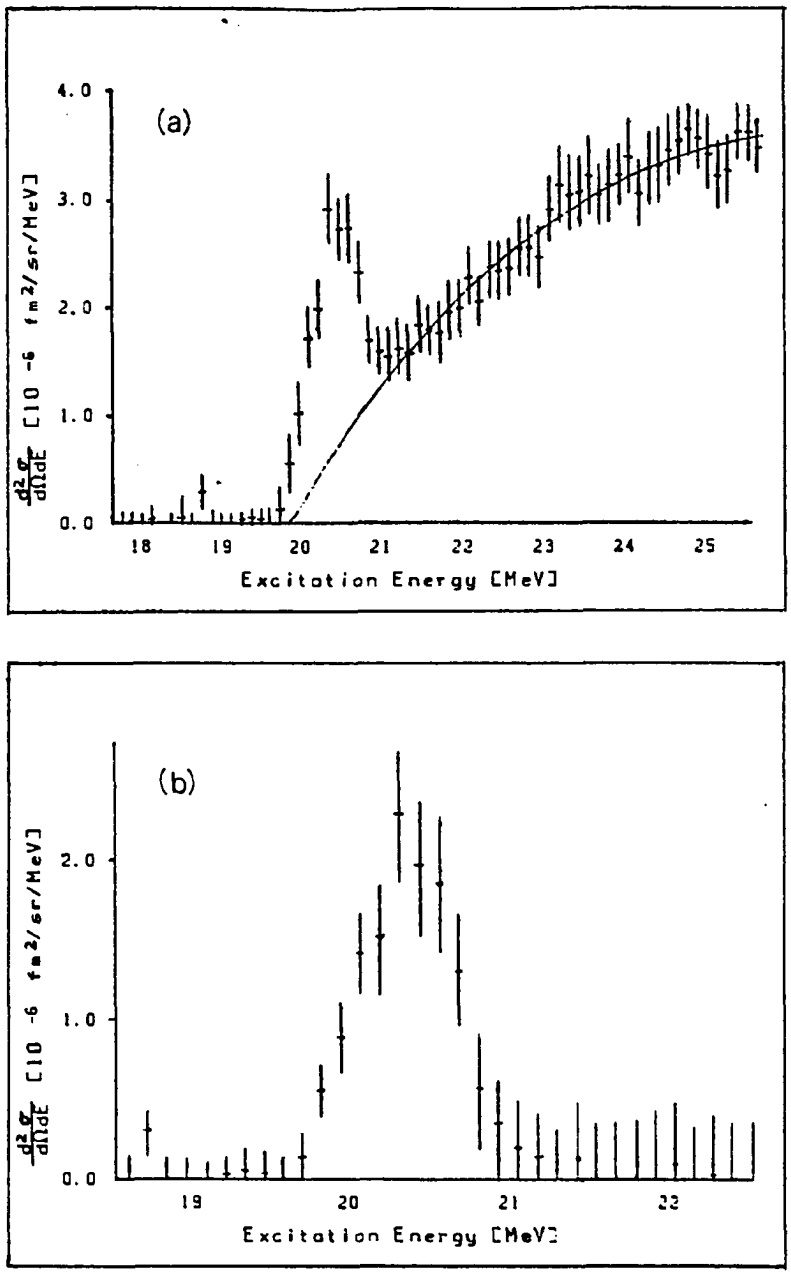

Figure 4. (a) Double-Differential Cross Section of The Break-Up Continuum With The Quasi-Bound-State Peak at an Incident Energy E_0 = 320 MeV and a Scattering Angle θ = 44.96°.
(b) Spectrum After Subtracting The Continuum Contribution.

(b) the spectrum after subtracting the continuum contribution (Kobschall et al., 1983).

The 0^+ state has been of interest for some time because inelastic electron scattering experiments (Kobschall et al., 1983; Frosch, Rand, Yearian, Crannell & Suelzle, 1968; Watcher, 1970) have shown that it accounts for a very small percentage of the energy weighted sum rule. The shell-model calculations which assum a $1s0s^{-1}$ ($J = 0$, $T = 0$) configuration have been demonstrated to over-predict the strength by a factor of 20 (Lui & Zamick, 1986). The inclusion of higher order shell model configurations can only reduce this factor to between 5 and 10. The exact nature of the 0^+ state is therefore considered to be somewhat puzzling and this has led to speculations that the shell model is inappropriate for describing this light system.

Two other types of calculations have been performed for this state. One is a resonating group calculation with a central interaction and bound state approximation (Furutani, Horiuchi, & Tamagaki, 1978). The resulting form factor was approximately three times larger than that observed. The other is a calculation employing hyperspherical harmonics (Samyal & Mukherjee, 1987). Here good agreement with the experiment form factor was obtained. Since the calculated state turned out to be a pure hyperradial excitation, the authors concluded that it was a collective excitation of the ground state.

The RCCSM in the 1p-1h approximations has been very successful in describing low energy nucleon scattering phenomena

for the four-nucleon systems (Halderson & Philpott, 1979). Previous attempts to describe inelastic scattering of pions and electrons in the context of the recoil corrected continuum shell model have considered only the coordinate r'_4 in figure 5 (Blilie et al., 1986), because the wave function for the coordinate ξ_3 is readily available. However, one sees that if the coordinate r'_4 is excited, the coordinates r'_1, r'_2, and r'_3 will also move slightly with respect to the center of mass. This constitutes a target recoil or center of mass correction which was omitted from previous work.

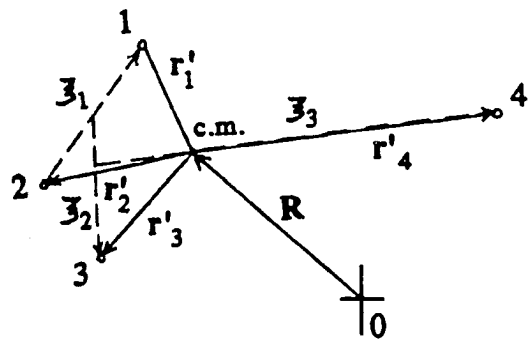

Figure 5. Internal Coordinates Within ^{4}He System.

Therefore, it is expected that 1p-1h RCCSM with full center of mass correction may provide an adequate description of the ^{4}He 0^+ state in a shell model context even for this light system.

In this work, the charge form factor of the 0^+ state of ^{4}He is calculated with RCCSM wave functions and with consideration of all the coordinate corrections. The result is compared with that obtained from experiments. It is found to be possible to describe the 0^+ state in a 1p-1h shell model context and a further work to improve the calculation is suggested.

Inelastic scattering cross section of 0^+–0^+ states in Born

approximation has a particularly simple form ($(q_\mu^2/2M_T^2)^2 \ll 1$, m = 0). from equation (1.11) one has

$$d\sigma/d\Omega = \{ 4\pi\sigma_m/[1+2E_1\sin^2(\theta/2)/M_T] \} \cdot \{[|\langle Y_f || \hat{M}_o^{coul}(q) || Y_i \rangle|^2]\}(q_\mu^4/q^4), \quad (1.16)$$

where

$$\sigma_M = \alpha^2\cos^2(\theta/2)/4E_1^2\sin^4(\theta/2). \quad (1.17)$$

The form factor is defined as

$$F(q^2) = (d\sigma/d\Omega)/4\pi Z^2\sigma_M. \quad (1.18)$$

The matrix elements $|\langle Y_f|| \hat{M}_o^{coul}(q) || Y_i \rangle|$ is calculated here by the recoil corrected continuum shell model.

CHAPTER II

DERIVATION OF CHARGE FORM FACTORS FOR ^{4}He

The recoil corrected continuum shell model employs the translationally invariant Hamiltonian

$$T + V = (2m)^{-1} \sum P^2 - T_{c.m.} + \sum_{i<j} V_{ij} , \qquad (2.1)$$

where the two-body interaction is the Coulomb potential plus the g-matrix interaction, M3Y (Bertsch, Borysowicz, McManus & Love, 1977), which includes noncentral forces. The basis consists of one-particle excitations in the harmonic oscillator wave functions for the internal coordinate ξ_3 in figure 6 Proper boundary conditions are imposed by R-matrix techniques at a matching radius of a_c = 7.2 fm. A smooth joining to Coulomb functions is accomplished by allowing particle excitations up to 2n + 1 = 14, where n begins at zero. The core states of ^{3}H and ^{3}He are taken as pure $0s^3$. The oscillator constant, v_o = mw/h, is chosen as 0.36 fm^{-2} to reproduce the mean-squared-radius of ^{3}H.

The great advantage of the RCCSM was its ability to provide matrix elements of translationally invariant operators in the internal coordinates by calculating matrix elements in normal shell model coordinates, r_i, with a fixed origin. This was very convenient for operators such as the two-body interaction, the kinetic energy, and transition operators for which a long wave-length approximation could be made. However, at high

momentum transfer, q, operators such as $j_1(qr'_1) = j_1(q|r_i\text{-}R|)$ do not lend themselves to a simple decomposition in terms of the shell model coordinates, r_i. Therefore the matrix element of interest for the present problem,

$$M_o = < Y_f \| \; Y_o \; (r'_i) \; j_o \; (qr'_i) \| \; Y_i > \qquad (2.2)$$

must be done explicitly in the relative coordinates.

Cross sections for excitation of states above particle emission threshold are given by the expression (Halderson, Philpott, Carr, and Petrovich, 1981)

$$d^2\sigma/d\Omega \, dE = (1/2\pi h^2)\sum_{c,J_B}(\mu_c/K_c)\cdot(d\sigma_{c,J_B}/d\Omega), \qquad (2.3)$$

where μ is the nucleon reduced mass, K_c is the nucleon asymptotic relative momentum in the channel c, and $d\sigma_{c,J_B}/d\Omega$ is a fictitious Born cross section, calculated for nucleon wave functions with flux V_c in channel c. The index c stands for $\alpha J_c j l$ with J_c and j coupled to J_B, where J_c is the angular momentum of ^3H or ^3He, l and j are the nucleon orbital and total angular momentum, and α distinquishes between ^3H and ^3He.

The form factor is calculated by equation (1.16) and (1.18). The Mott cross section, σ_M is given by (1.17).

To calculate the reduced matrix elements in equation (1.16), one needs the wave functions of the initial and final states. The ground state of ^4He here is still approximated by a pure $0s^4$,

$$Y_i = a_o \; | \; 0s^4 > | \; s = 0 > , \qquad (2.4)$$

where $a_o = 1$, but all coordinates are considered. The final is a linear combination of states of the form

$$Y_f = A_\tau \; \{[0s_{1/2}{}^3(\xi_i)\cdot nlj \; (\xi_3)]^{J_f}_{M_f} O_s(R)\} \; , \qquad (2.5)$$

where $A_\tau = [2(1+d)]^{-1/2}\ (1 - P_{ij}^{\tau})$, and ξ_i is the internal coordinates.

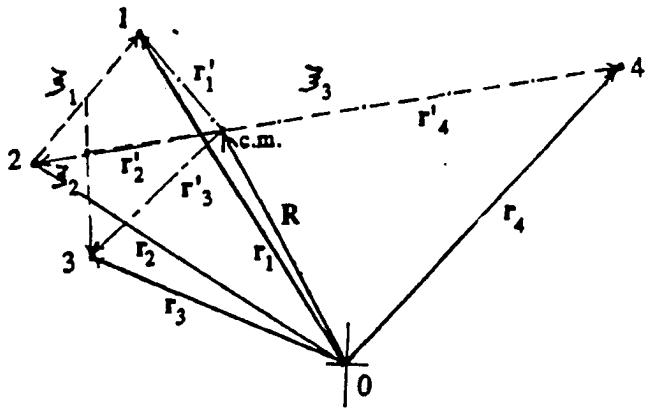

Figure 6. Coordinate Transformation Within ^{4}He System.

Consider the initial state Y_i first, it can be decomposed into space and spin parts:

$$Y_i = Y_{ispace} \cdot X_{ispin}. \tag{2.6}$$

For Y_{ispace}, it is taken as

$$Y_{ispace} = (v_o/\pi)^3 \exp\{(-v_o/2)(r_1^2 + r_2^2 + r_3^2 + r_4^2)\}$$

or

$$Y_{ispace} = (v_o/\pi)^3 \exp\{(-v_o/2)(4R^2 + r_1'^2 + r_2'^2 + r_3'^2 + r_4'^2)\}\ . \tag{2.7}$$

To convert Y_{ispace} into the internal coordinates ξ_i, one uses the transformation

$$r_1'^2 = \xi_3^2/16 + \xi_2^2/9 + \xi_1^2/4 + \xi_3\cdot\xi_2/6 - \xi_3\cdot\xi_1/4 - \xi_2\cdot\xi_1/3$$

$$r_2'^2 = \xi_3^2/16 + \xi_2^2/9 + \xi_1^2/4 + \xi_3\cdot\xi_2/6 + \xi_3\cdot\xi_1/4 + \xi_2\cdot\xi_1/3$$

$$r_3'^2 = \xi_3^2/16 + 4\xi_2^2/9 - \xi_3\cdot\xi_2/3$$

$$r_4'^2 = 9\xi_3^2/16.$$

Since

$$r_1'^2 + r_2'^2 + r_3'^2 + r_4'^2 = 3\xi_3^2/4 + 2\xi_2^2/3 + \xi_1^2/2 \tag{2.8}$$

Then

$$Y_{ispace} = (v_o/\pi)^3 \exp\{-(v_o/2)(4R^2 + 3\xi_3^2/4 + 2\xi_2^2/3 + \xi_1^2/2) \}$$
$$= (4v_o/\pi)^{3/4} \exp\{-(1/2)(4v_o)R^2\}$$
$$\cdot(3v_o/4\pi)^{3/4} \exp\{-(1/2)(3v_o/4)\xi_3^2\}$$
$$\cdot(2v_o/3\pi)^{3/4} \exp\{-(1/2)(2v_o/3)\xi_2^2\}$$
$$\cdot(v_o/2\pi)^{3/4}\exp\{-(1/2)(v_o/2)\xi_1^2\}$$
$$= O_s^{4v_o}(R)O_s^{3v_o/4}(\xi_3)O_s^{2v_o/3}(\xi_2)O_s^{v_o/2}(\xi_1). \quad (2.9)$$

Since both neutron and proton are spin 1/2 particles, which have only two eigen-functions $X_+(1/2)$ and $X_-(1/2)$, the function X_{ispin} is antisymmetric between neutrons or between protons. Therefore it has the form

$$X = 2^{-1/2}(X_+^{(1)}X_-^{(2)} - X_-^{(1)}X_+^{(2)}) \quad (2.10)$$

for neutrons and protons. So, X_{ispin} is written as

$$X_{ispin} = [\, 2^{-1/2}(X_+^{(1)}X_-^{(2)} - X_-^{(1)}X_+^{(2)})]_p$$
$$\cdot [\, 2^{-1/2}(X_+^{(1)}X_-^{(2)} - X_-^{(1)}X_+^{(2)})]_n . \quad (2.11)$$

For final state Y_f, one of the nucleons is excited so that Y_f now is expressed as a linear combination of 1p-1h states,

$$Y_f = Y_{fspace} \cdot X_{fspin} . \quad (2.12)$$

where

$$Y_{fspace} = A_\tau O_s^{4v}(R)\psi(\xi_3)O_s^{2v/3}(\xi_2)O_s^{v/2}(\xi_1) . \quad (2.13)$$

Here, $\psi(\xi_3)$ is the final spatial wave function of excited nucleon.

To determine the normalization of this 1p-1h state, it is the best to choose LS coupling for Y_{fspace}. Refering on s to figure 7, one has all the core orbital numbers zero and total spin $[2^{-1} \otimes 2^{-1}]^o \otimes 2^{-1}(2^{-1})$, while the excited neutron or proton's numbers are l, S =1/2, j. Here

$$O_{S1/2}{}^3{}_{ms} = O_s(\xi_1)O_s(\xi_2)[\ 2^{-1/2}\ (X_+^{(1)}X_-^{(2)}-X_-^{(1)}X_+^{(2)})]_{p\text{ or }n}\cdot X_{ms\ n\text{ or }p}$$

and

$$Y_f = A_{\mathcal{T}}\,(-1)^{1/2+j-Jf}\sum_{s}(-1)^{l+1/2+1/2+Jf}\,\hat{s}\cdot\hat{j}\begin{Bmatrix} l & \frac{1}{2} & j \\ \frac{1}{2} & J_f & s \end{Bmatrix}$$
$$\cdot\ \{\ nl^{\mathcal{T}}(\xi_3)[1/2,1/2]^s(J_f)O_s(R)\ \} \qquad (2.15)$$

where $\hat{s} = (2s+1)^{1/2}$, $\sum_s$ is the summation over s = 0 and 1,

$$[1/2,\ 1/2]^o = [2^{-1/2}(X_+^{(1)}X_-^{(2)}-X_-^{(1)}X_+^{(2)})_p]$$
$$\cdot\ [2^{-1/2}(X_+^{(1)}X_-^{(2)}-X_-^{(1)}X_+^{(2)})_n], \qquad (2.16)$$

and

$$[1/2,\ 1/2]^{s=1}{}_{Ms=0} = [2^{-1/2}(X_+^{(1)}X_-^{(2)}-X_-^{(1)}X_+^{(2)})_p]$$
$$\cdot\ [2^{-1/2}(X_+^{(1)}X_-^{(2)}+X_-^{(1)}X_+^{(2)})_n]. \qquad (2.17)$$

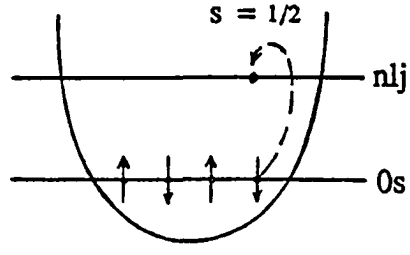

Figure 7. Spin Coupling For The Core of $^4He(0^+)$.

The state Y_f becomes

$$A_{\mathcal{T}}\{nl^{\mathcal{T}}(\xi_3)(1/2,1/2)^o(1)\}O_S(R)$$
$$= [2(1+d)]^{-1/2}\{(1\ -\ P_{34})$$
$$\cdot\psi_{n\,l}(3v/4\ ;\xi_3)O_S(2v/3\ ;\xi_2)O_S(v/2\ ;\xi_1)|S=0>\}O_S(R)$$
$$= [2(1+d)]^{-1/2}\{\psi_{n\,l}(\xi_3)O_S(\xi_2)O_S(\xi_1)$$
$$+\psi_{n\,l}(4r'_3/3)O_S(3r'_4/2+r'_3/2)O_S(\xi_1)\}|S=0>O_S(R) \qquad (2.18)$$

Let $$D = \psi_{n\,l}(\xi_3)O_S(\xi_2)O_S(\xi_1) \qquad (2.19)$$

$$E = \psi_{n\,l}(4r'_3/3)O_S(3r'_4/2+r'_3/2)O_S(\xi_1) \qquad (2.20)$$

then

$$< Y_f |\ Y_f > = 1 = [2(1+d)]^{-1}\{1+1+2<D|E>\} \qquad (2.21)$$

and

$$d = \langle D|E \rangle$$
$$= \int \psi_{n\,l}^{*}(\xi_3) O_S(\xi_2) O_S(\xi_1) \cdot \psi_{n\,l}(4r'_3/3) O_S(3r'_4/2 + r'_3/2) O_S(\xi_1) d\xi_1 d\xi_2 d\xi_3$$
$$= \int \psi_{n\,l}^{*}(4r'_4/3) O_S(3r'_3/2 + r'_4/2) \cdot \psi_{n\,l}(4r'_3/3) O_S(3r'_4/2 + r'_3/2) d\xi_2 d\xi_3$$
$$= \int \psi_{n\,l}^{*}(\xi_3) O_S(\xi_2) \psi_{n\,l}(-\xi_3/3 + 8\xi_2/9) O_S(\xi_3 + \xi_2/3) d\xi_2 d\xi_3 \qquad (2.22)$$

Let

$$y = \xi_3 ,$$
$$x = 8\xi_2/9 - \xi_3/3 ,$$

then

$$\xi_3 = y ,$$
$$\xi_2 = 9(x + y/3)/8 ,$$

and

$$J = \partial(\xi_2, \xi_3)/\partial(x, y) = \begin{vmatrix} 9/8 & 0 \\ 3/8 & 1 \end{vmatrix} = 9/8 ,$$

therefore

$$\langle D|E \rangle = (9/8)^3 \int \psi_{nl}^{*}(y) O_s(3y/8 + 9x/8) \cdot \psi_{nl}(x) O_s[y + (3y/8 + 9x/8)/3] dx dy$$
$$= (9/8)^3 \int \psi_{nl}^{*}(y) O_s(3y/8 + 9x/8) \cdot \psi_{nl}(x) O_s(9y/8 + 3x/8) dx dy$$
$$= (9/8)^3 (2v/3\pi)^{3/2} \int \psi_{nl}^{*}(y) \exp\{-(v/3)(3y/8 + 9x/8)^2\} \cdot \psi_{nl}(x) \exp\{-(v/3)(9y/8 + 3x/8)^2\} dx dy$$
$$= (9/8)^3 (2v/3\pi)^{3/2} \int \psi_{nl}^{*}(y) \exp\{-(3v/64)(y + 3x)^2\} \cdot \psi_{nl}(x) \exp\{-(3v/64)(3y + x)^2\} dx dy$$

Let $z = -x$, $dz = |J| dx$, then

$$\begin{aligned}\langle D|E\rangle &= (9/8)^3(2v/3\pi)^{3/2}\int\psi_{nl}^*(y)\exp\{-(3v/64)(4y^2+4z^2-12y\cdot z)\}\\ &\quad\cdot\psi_{nl}(x)dzdy\\ &= (9/8)^3(2v/3\pi)^{3/2}\int\psi_{nl}^*(y)\exp\{-(9v/32)(y^2+z^2-2y\cdot z)\\ &\quad+v(y^2+z^2)/4\}\psi_{nl}(x)dzdy\\ &= (-1)^l(9/8)^3(2v/3\pi)^{3/2}\int\psi_{nl}^*(y)\exp\{-(9v/32)(y-z)^2\}\\ &\quad\cdot\exp\{3v(y^2+z^2)/32\}\psi_{nl}(z)dzdy\end{aligned} \tag{2.23}$$

Expansion of $\exp\{-r(a-b)\}$ is:

$$\exp\{-r(a-b)\} = \sum_l (i)^{-l}(2l+1)\exp\{-r(a^2+b^2)j_l(i2rab)\cdot C_l(O_aY_a)C_l(O_bX_b)$$

where, $C_{lm} = [4\pi/(2l+1)]Y_{lm}$.

Then

$$\exp\{-r(a-b)\} = \sum_l (i)^{-l}(2l+1)\exp\{-r(a^2+b^2)j_l(i2rab)\cdot[4\pi/(2l+1)]\ Y_{lm}^*\,Y_{lm}\,.$$

Therefore

$$\exp\{-9v(y-z)^2/32\} = \sum_l (i)^{-l}4\pi\cdot\exp\{-9v(y^2+z^2)/32\}\cdot j_l(i9vyz/16)Y_{lm}^*(z)Y_{lm}(y)\,. \tag{2.24}$$

Substituting equation (2.24) into equation (2.23), one has

$$\begin{aligned}\langle D|E\rangle &= (-1)^l(9/8)^3(2v/3\pi)^{3/2}(4\pi)\int R_{nl}(y)\ i^{-l}\\ &\quad\cdot\exp\{-15v(y^2+z^2)/32\}j_l(9ivyz/16)R_{nl}(z)z^2y^2dzdy\ .\end{aligned} \tag{2.25}$$

Once the norm of the excited state is determined one can calculate matrix elements of operators connecting to the ground state. For reduced matrix elements of operators not a function of spin, one may discard the s = 1 component of the excited state. We take

$$\psi^{J_f}_{Mf} = (-1)^{l-1/2+j}\hat{j}\begin{Bmatrix} l & \frac{1}{2} & j \\ \frac{1}{2} & J_f & s \end{Bmatrix} A_\tau\{nl^\tau(\xi_3)[1/2,1/2]^o(J_f)O_s(R)\}$$

$$= (-1)^{l-1/2+j+1/2+l+j}(j/2^{1/2}l)A_\tau\{nl^\tau(\xi_3)[1/2,1/2]^o(J_fM_f)O_s(R)$$

$$= -(j/2^{1/2}l)[2(1+d)]^{-1/2}\{\psi_{nl}(\xi_3)O_s(\xi_2)O_s(\xi_1)$$

$$+\psi_{nl}(3r'_3/4)O_s(3r'_4/2+r'_3/2)O_s(\xi_1)\}|S=0>O_s(R).$$

Here, $\hat{j} = (2j+1)^{1/2}$.

The charge form factor must now be calculated as the transition matrix element between the initial and final states. The matrix elements have the form $< Y_f | O^k | Y_i > = < D+E | O^k | 0 >$, where

$$O^k = O_1^k(r'_1,\alpha) + O_2^k(r'_2,\alpha) + O_3^k(r'_3,\beta) + O_4^k(r'_4,\beta), \quad (2.26)$$

$\alpha \sim$ proton ,

$\beta \sim$ neutron ,

and for Coulomb form factor here, $O_i^k(r'_i,\tau_i) = c_\tau j_k(q\, r'_i)Y_{kQ}(r'_i)$. Since Y_f and $| 0 >$ are antisymmetric in exchanging the neutrons or exchanging the protons, then

$$< Y_f | O_1+O_2 | 0 > = 2< Y_f | O_1 | 0 >,$$

and

$$< Y_f | O_3+O_4 | 0 > = 2< Y_f | O_4 | 0 >.$$

First look at (with $v \longrightarrow 3v_o/4$ for the state ψ_{nl})

$$< D | O_4 | 0 > \sim \int \psi_{nl}^*(\xi_3)O_s(\xi_2)O_s(\xi_1)O_s(R)O_4^k(3\xi_3/4)$$

$$\cdot\, O_s(\xi_3)O_s(\xi_2)O_s(\xi_1)O_s(R)d\xi_1 d\xi_2 d\xi_3 dR$$

$$= \int \psi_{nl}^*(\xi_3)O_4^k(3\xi_3/4)O_s(\xi_3)d\xi_3 \quad (2.27)$$

Second look at

$$< E | O_4 | 0 > \int \psi_{nl}^*(-\xi_3/3+8\xi_2/9)O_s(\xi_3+\xi_2/3)$$

$$\cdot\, O_4^k(3\xi_3/4)O_s(\xi_3)O_s(\xi_2)d\xi_2 d\xi_3. \quad (2.28)$$

Again

$$y = \xi_3 ,$$

$$x = 8\xi_2/9 - \xi_3/3 ,$$

then

$$\xi_3 = y ,$$

$$\xi_2 = 9(x + y/3)/8 ,$$

and

$$J = \partial(\xi_2,\xi_3)/\partial(x, y) = \begin{vmatrix} 9/8 & 0 \\ 3/8 & 1 \end{vmatrix} = 9/8$$

Therefore

$$\begin{aligned} <E \mid O_4 \mid 0> &\sim (9/8)^3 \int \psi_{nl}^*(x) O_s[y+(3y/8+9x/8)/3] \\ &\quad \cdot O_4^k(3y/4) O_s(3y/4) O_s(3y/8+9x/8) dx dy \\ &= (9/8)^3 \int \psi_{nl}^*(x) O_s(9y/8+3x/8) \\ &\quad \cdot O_4^k(3y/4) O_s(3y/4) O_s(3y/8+9x/8) dx dy \\ &= (9/8)^3 \int \psi_{nl}^*(x) (2v/3\pi)^{3/2} \\ &\quad \cdot \exp\{-(3v/64)(4y^2+4x^2-12y\cdot x)\} \\ &\quad \cdot O_4^k(3y/4) O_s(3y/4) dx dy \\ &= (9/8)^3 \int \psi_{nl}^*(x) (2v/3\pi)^{3/2} \\ &\quad \cdot \exp\{-(18v/64)(y^2+x^2+2y\cdot x)\} \\ &\quad \cdot \exp\{(3v/32)(y^2+x^2)\} \\ &\quad \cdot O_4^k(3y/4) O_s(3y/4) dx dy \\ &= (9/8)^3 \int \psi_{nl}^*(x) (2v/3\pi)^{3/2} \exp\{-(9v/32)(y+x)^2\} \\ &\quad \cdot \exp\{(3v/32)(y^2+x^2) O_4^k(3y/4) O_s(3y/4) dx dy \\ &= (-1)^l (9/8)^3 (2v/3\pi)^{3/2} (4\pi) \int R_{nl}(x)\, i^{-l} \cdot \\ &\quad \cdot \exp\{-3v(y^2+x^2)/16\} \\ &\quad \cdot j_l(9ivyx/16) O_4(3y/4) O_s(3y/4) x^2 y^2 dx dy \end{aligned} \tag{2.29}$$

where

$$O_4^k(3y/4) = O(3y/4)Y_{lm}(y) . \qquad (2.30)$$

Therefore

$$\begin{aligned} <Y_f | O_4^k | 0> &= <Y_{Mf} | O_4^k Q | 0> \\ &= -(\hat{j}/2^{1/2}\hat{I})[2(1+d)]^{-1/2} \\ &\{\int R_{nl}^{3v/4}(\xi_3) O_4(3\xi_3/4) O_s(\xi_3)\xi_3^2 d\xi_3 \\ &+ (-1)^l (9/8)^3 (2v/3\pi)^{3/2}(4\pi)\int R_{nl}(x)\, i^{-l} \\ &\cdot \exp[-3v(y^2+x^2)/16 j_l(9ivyx/16) \\ &\cdot O_4(3y/4) O_s(3y/4) x^2 y^2 dx dy\} . \end{aligned} \qquad (2.31)$$

$$<D | O_4 | 0> \sim \int \psi_{nl}^*(\xi_3) O_s(\xi_2) O_s(\xi_1) O_1(r'_1) O_s(\xi_3) O_s(\xi_2) O_s(\xi_1) d\xi_1 d\xi_2 d\xi_3 .$$

Therefore

$$<D | O_1(r'_1) | 0> = <D | O_1(r'_3) | 0>$$

$$<E | O_1 | 0> \sim \int \{P_{34}[\psi_{nl}^*(\xi_3) O_s(\xi_2) O_s(\xi_1) O_s(\xi_1)]\} O_1(r'_1) O_s(\xi_3) O_s(\xi_2) O_s(\xi_1) d\xi_1 d\xi_2 d\xi_3$$

$$<E | O_1 | 0> = <E | O_1(r'_4) | 0> = (\text{ in fact }) <D | O_1(r'_3) | 0> .$$

Therefore

$$<D+E | O_1 | 0> = 2<D | O_1(r'_3) | 0> \sim \int \psi_1^*(4r'_4/3) O_s(3r'_3/2+r'_4/2) O_1(r'_3) O_s(4r'_4/3) O_s(3r'_3/2+r'_4/2) d\xi_2 d\xi_3 \qquad (2.32)$$

Let

$$\xi_3 = 4r'_4/3 ,$$

$$\xi_2 = 3r'_3/2+r'_4/2 ,$$

then

$$\partial(\xi_2\xi_3)/\partial(r_3' r_4') = \begin{vmatrix} 3/2 & 0 \\ 1/2 & 4/3 \end{vmatrix} = 2 .$$

Therefore

$$
\begin{aligned}
&< D+E \mid O_1 \mid 0 > = 2< D \mid O_1(r'_3) \mid 0 > \\
&\quad \sim 8\int \psi_{nl}^*(4r'_4/3)(2v/3\pi)^{3/2} \\
&\qquad \cdot \exp\{-v(3r'_3/2+r'_4/2)^2/3\} O_1(r'_3) O_s(4r'_4/3) dr'_3 dr'_4 \\
&\quad = 8\int \psi_{nl}^*(4r'_4/3)(2v/3\pi)^{3/2} \\
&\qquad \cdot \exp\{-v(3r'_3+r'_4)^2/6\} O_1(r'_3) O_s(4r'_4/3) dr'_3 dr'_4 \\
&\quad = 8\,(2v/3\pi)^{3/2}\int \psi_{nl}^*(4\pi) i^{-l} \exp\{-v(9r'^2_3+ r'^2_4)^2/6\} j_l(ivr'_3 r'_4) \\
&\qquad \cdot Y_{lm}^*(r'_3) Y_{lm}^*(r'_4) O_1(r'_3) O_s(4r'_4/3) dr'_3 dr'_4 \\
&\quad = 32\pi(2v/3\pi)^{3/2}\, i^{-l}\int R_{nl}(4\, r'_4/3) \exp\{-v(9r'^2_3+ r'^2_4)^2/6\} \\
&\qquad \cdot (-1)^l j_l(ivr'_3 r'_4) O(r'_3) O_s(4r'_4/3) r'^2_3 r'^2_4 dr'_3 dr'_4 \ .
\end{aligned}
\tag{2.33}
$$

Therefore

$$
\begin{aligned}
&< Y_f \mid O_1 \mid 0 > = -2(\hat{j}/2^{1/2}\hat{l})[2(1+d)]^{-1/2} \\
&\qquad \{\, 32\pi(2v/3\pi)^{3/2}\, i^{-l}\int R_{nl}(4r'_4/3) \\
&\qquad\quad \cdot \exp[-v(9r'^2_3+r'^2_4)^2/6](-1)^l j_l \\
&\qquad\quad \cdot (ivr'_3 r'_4) O(r'_3) O_s(4r'_4/3) r'^2_3 r'^2_4 dr'_3 dr'_4 \}.
\end{aligned}
\tag{2.34}
$$

And

$$
\begin{aligned}
&< Y_f^{kQ} \mid O_1+O_2+O_3+O_4 \mid 0 > \\
&\quad = -2(\hat{j}/2^{1/2}\hat{l})[2(1+d)]^{-1/2} \cdot \{\int R_{nl}{}^{3v/4}(\xi_3)\, O_4(3\xi_3/4) O_s(\xi_3) \xi_3^2 d\xi_3 \\
&\qquad +4\pi(2v/3\pi)^{3/2}(-l)^l \cdot [(9/8)^3\int R_{nl}(x)\, i^{-l} \\
&\qquad \cdot \exp\{-15v(y^2+x^2)/32\} j_l(9ivyx/16) O_4(y) O_s(3y/4) x^2 y^2 dxdy \\
&\qquad\quad + 16\int R_{nl}(4r'_4/3) \exp\{-v(9r'^2_3+r'^2_4)^2/6\}\, i^{-l} \\
&\qquad\qquad \cdot j_l(ivr'_3 r'_4) O(r'_3) O_s(4r'_4/3) r'^2_3 r'^2_4 dr'_3 dr'_4] \}. \\
&\quad = -2(\hat{j}/2^{1/2}\hat{l})[2(1+d)]^{-1/2}\{ME(1)+ME(2)+ME(3)\}
\end{aligned}
\tag{2.35}
$$

where

$$ME(1) = \int R_{nl}{}^{3v/4}(\xi_3)O_4(3\xi_3/4)O_s(\xi_3)\xi_3{}^2 d\xi_3 , \qquad (2.36)$$

$$ME(2) = 4\pi(2v/3\pi)^{3/2}(-1)^l(9/8)^3 \cdot \int R_{nl}(x)\, i^{-l} \exp\{-15v(y^2+x^2)/32\} \cdot j_l(9ivyx/16)O_4(y)O_s(3y/4)x^2y^2dxdy , \qquad (2.37)$$

$$ME(3) = 4\pi(2v/3\pi)^{3/2}(-1)^l \cdot 16 \cdot \int R_{nl}(4r'_4/3)\exp[-v(9r'_3{}^2 + r'_4{}^2)^2/6] \cdot i^{-l}j_l(ivr'_3\, r'_4)O(r'_3)O_s(4r'_4/3)r'_3{}^2r'_4{}^2dr'_3dr'_4 . \qquad (2.38)$$

and

$$d = \langle D|E\rangle = (-1)^l(9/8)^3(2v/3\pi)^{3/2}(4\pi)\int R_{nl}(y)\, i^{-l} \exp\{-15v(y^2+z^2)/32\} \cdot j_l(9ivyz/16)R_{nl}(z)z^2y^2dzdy . \qquad (2.39)$$

Equation (2.35) is the transition matrix element between the initial and final states of the nucleus. Here, if the all coordinates had not been considered, equations (2.37) and (2.38) would not have appeared in (2.35).

CHAPTER III

THE CALCULATION AND THE RESULTS

As mentioned in Chapter II, the calculation of charge form factor has been deduced as determing the transition matrix elements between the initial and final states by equation (2.33), or

$$
\begin{aligned}
&<Y_f^k{}_Q|\, O_1+O_2+O_3+O_4\,|0> \\
&\quad = -2(\hat{j}/2^{1/2}\hat{1})[2(1+d)]^{-1/2}\cdot\Big\{\int R_{nl}{}^{3v/4}(\xi_3)O_4(3\xi_3/4)O_s(\xi_3)\xi_3{}^2 d\xi_3 \\
&\qquad +4\pi(2v/3\pi)^{3/2}(-1)^l\cdot[(9/8)^3\int R_{nl}(x)\, i^{-l}\exp\{-15v(y^2+x^2)/32\} \\
&\qquad\qquad \cdot j_l(9ivyx/16)O_4(y)O_s(3y/4)x^2y^2dxdy \\
&\qquad\qquad +16\int R_{nl}(4r'_4/3)\exp\{-v(9r'_3{}^2+ r'_4{}^2)^2/6\}i^{-l} \\
&\qquad\qquad j_l(ivr'_3\, r'_4)O(r'_3)O_s(4r'_4/3)r'_3{}^2r'_4{}^2dr'_3dr'_4]\Big\} \\
&\quad = -2(\hat{j}/2^{1/2}\hat{1})[2(1+d)]^{-1/2}\ \{\ ME(1) + ME(2) + ME(3)\ \}\ ,
\end{aligned}
\tag{3.1}
$$

where ME(1) is given by equation (2.36), ME(2) is by (2.37), ME(3) is by (2.38), and d = <D|E> is by (2.39). In the calculating,

$$
\begin{aligned}
O_4(3\xi_3/4) &= j_0(3\xi_3 q/4)/(4\pi)^{-1/2}, \\
O_s(\xi_3) &= R_{os}{}^{(3/4)}(\xi_3)/(4\pi)^{-1/2}, \\
O_4(3y/4) &= j_0(3yq/4)/(4\pi)^{-1/2}, \\
O_s{}^{3/4}(y) &= R_{os}{}^{(3/4)}(y)/(4\pi)^{-1/2}, \\
O(r_3{}^1) &= j_o(r_3{}^1 q)/(4\pi)^{-1/2}, \\
O_s{}^{3/4}(4r_4{}^1/3) &= R_{os}{}^{(3/4)}(4r_4{}^1/3)\cdot(4\pi)^{-1/2}.
\end{aligned}
$$

All the calculations are done by computer. First of all, the

evaluation of $d = < D| E >$ is carried out. In actual calculating of the present problem, $l = 0$, $n = 1, \ldots, 7$,

$$\begin{aligned} j_1(9ivyz/16) &= j_0(9ivyz/16) \\ &= (16/i9vyz) \cdot \sin(i9xyz/16) \\ &= (16/i9vyz) \cdot (\exp\{-9vyz/16\} - \exp\{9vyz/16\})/2i, \\ &= -(8/9vxz) \cdot (\exp\{-9vyz/16\} - \exp\{9vyz/16\}) \end{aligned} \tag{3.2}$$

while $v_o = mv/h = 0.36 fm^{-2}$, and q ranges from 0.0 to 3.0 fm^{-1}. The two-dimensional integrals are evaluated by Simpson's rule in each dimension. The integration over y and z from 0.0 to 8.0 fm, 0.0 to 10.0 fm, and 0.0 to 12.0 fm are performed respectively, with total 170 integral subintervals. Since the integral value of <D|E> does not change significantly from an upper limit of 10.0 fm to one of 12.0 fm, the actual computing is then carried out by setting the up limit of 12.0 fm for both y and z.

Second, ME(1), ME(2) and ME(3) are computed for n = 1,2, 3, 4, 5, 6, 7, respectively. Figure 8 shows the results of ME(1). Here one can see that for values of $q < 2$ fm^{-1}, one need only consider particle excitations with $n \leq 5$. The results of ME(3) are shown in figures 9, 10, and 11. ME(3) along with ME(2) are the terms contributing to the target recoil correction. As one can see in the figure 9 to 11, strength of ME(3) contribution for n = 2 drops to very weak, and for $n \geq 3$, ME(3) becomes negligible. Therefore convergence in n is very fast for ME(3). Similar results are obtained for ME(2).

Next, the equation (3.1) is taken into equations (1.13) and

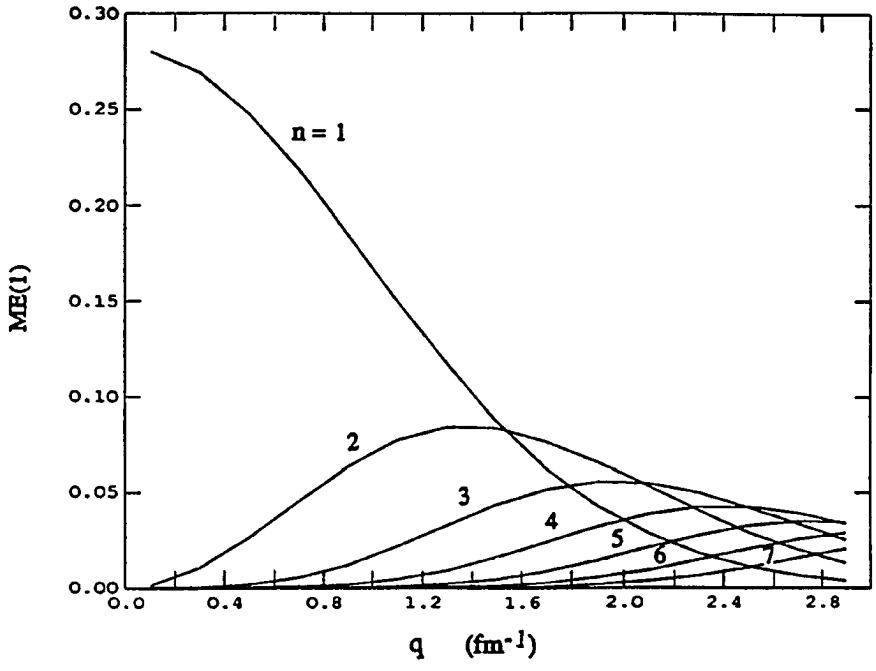

Figure 8. ME(1) vs. q for n = 1, 2, 3, 4, 5, 6, 7

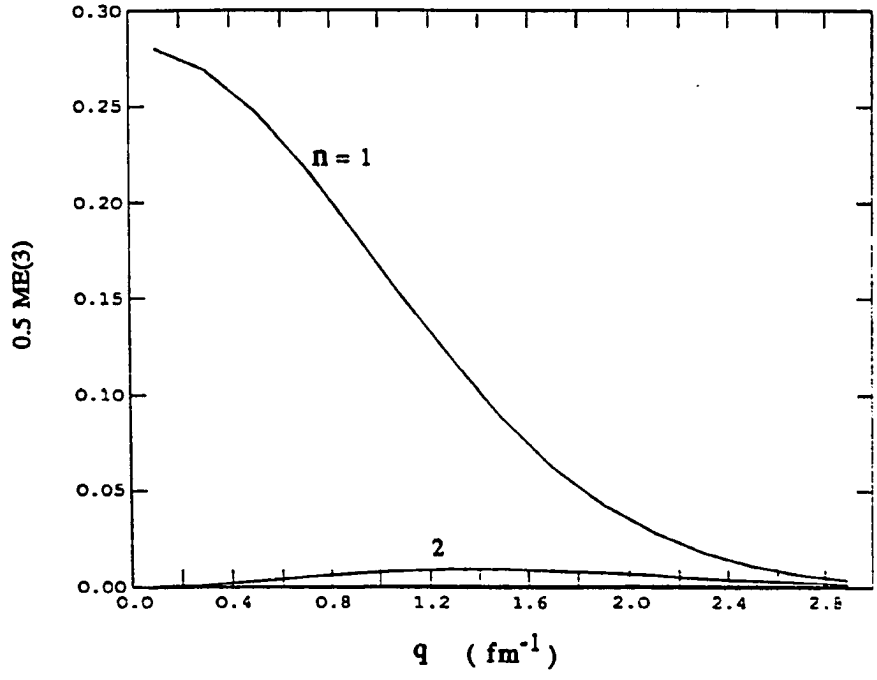

Figure 9. 0.5 ME(3) vs. q for n = 1, 2

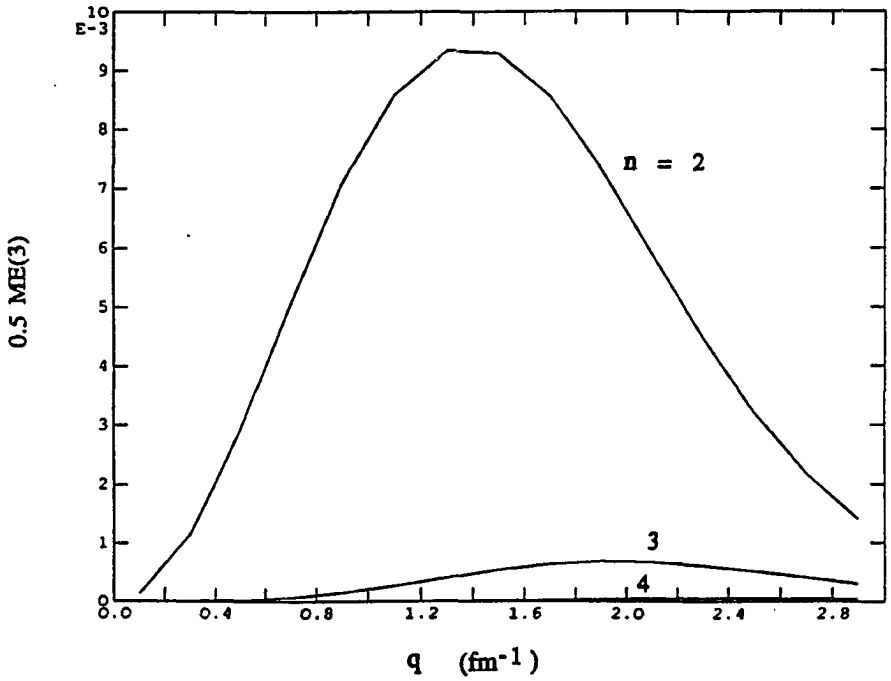

Figure 10. 0.5 ME(3) vs. q for n = 2, 3, 4

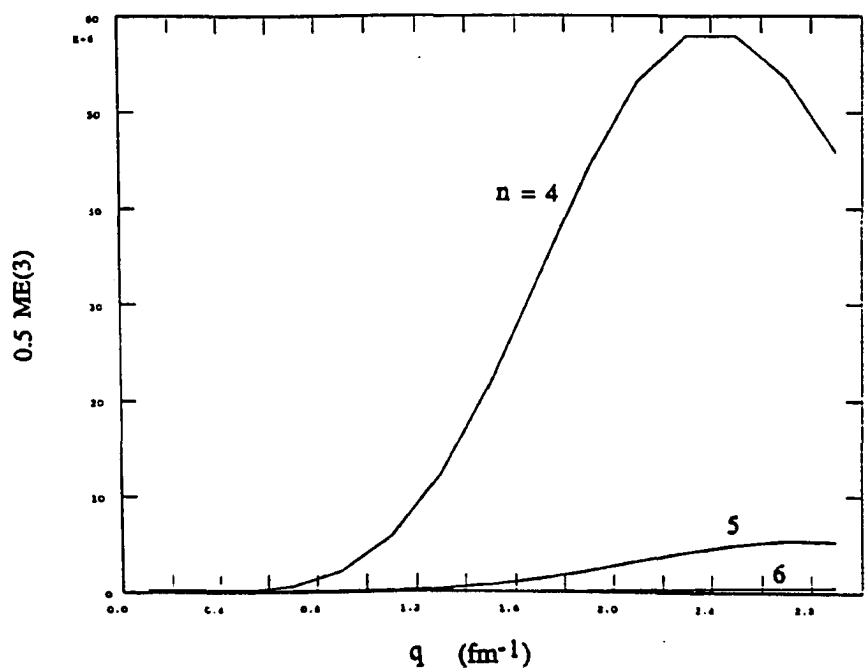

Figure 11. 0.5 ME(3) vs. q for n = 4, 5, 6

(1.15) for computing form factors as a function of q and E_p. The excitation energy range of interest is E_p = 0.0 – 1.20 MeV. Coefficients in the expansion $\psi_f = \sum_n a_n Y_f(n)$ are taken from the work of Halderson and Philpott, 1976; and are a function of the excitation energy. The n = 0 terms are eliminated from the final wave function to maintain orthogonality with the $0s^4$ ground state.

The reason for choosing E_p = 0.0 – 1.20 MeV is for convenience sake of comparing the final result with experimental data (Frosch, Rand, Yearian, Crannell & Suelzle, 1965; Walcher, 1970; Kobschall et al. 1983). There, the data was integrated from around 19.8 to about 21.0 MeV. (See figure 4.)

Figure 12 shows the form factors as a function of q and E_p. Here one sees that part of the resonance appears to be cut away, and the resonance is placed at a slightly higher location (19.8 + 0.7 = 20.5 MeV) than that of observed. The begining of the resonance cut coincides with the opening of the neutron threshold. With no Coulomb barrier the s-wave neutron escapes easily and produces a very broad resonance. This asymmetric shape was predicted from the work of Crone and Werntz (1967). The latter is caused by the slightly higher location prediction of the M3Y interaction for the 0^+ resonance, and the neutron threshold is calculated to be 0.69 MeV instead of 0.76 MeV as observed experimentally.

Lastly, figure 13 shows two calculated form factors $F(q^2)$ with the form factor extracted from experiments (Frosch, Rand, Yearian, Crannell & Suelzle, 1965; Walcher, 1970; Kobschall et al., 1983).

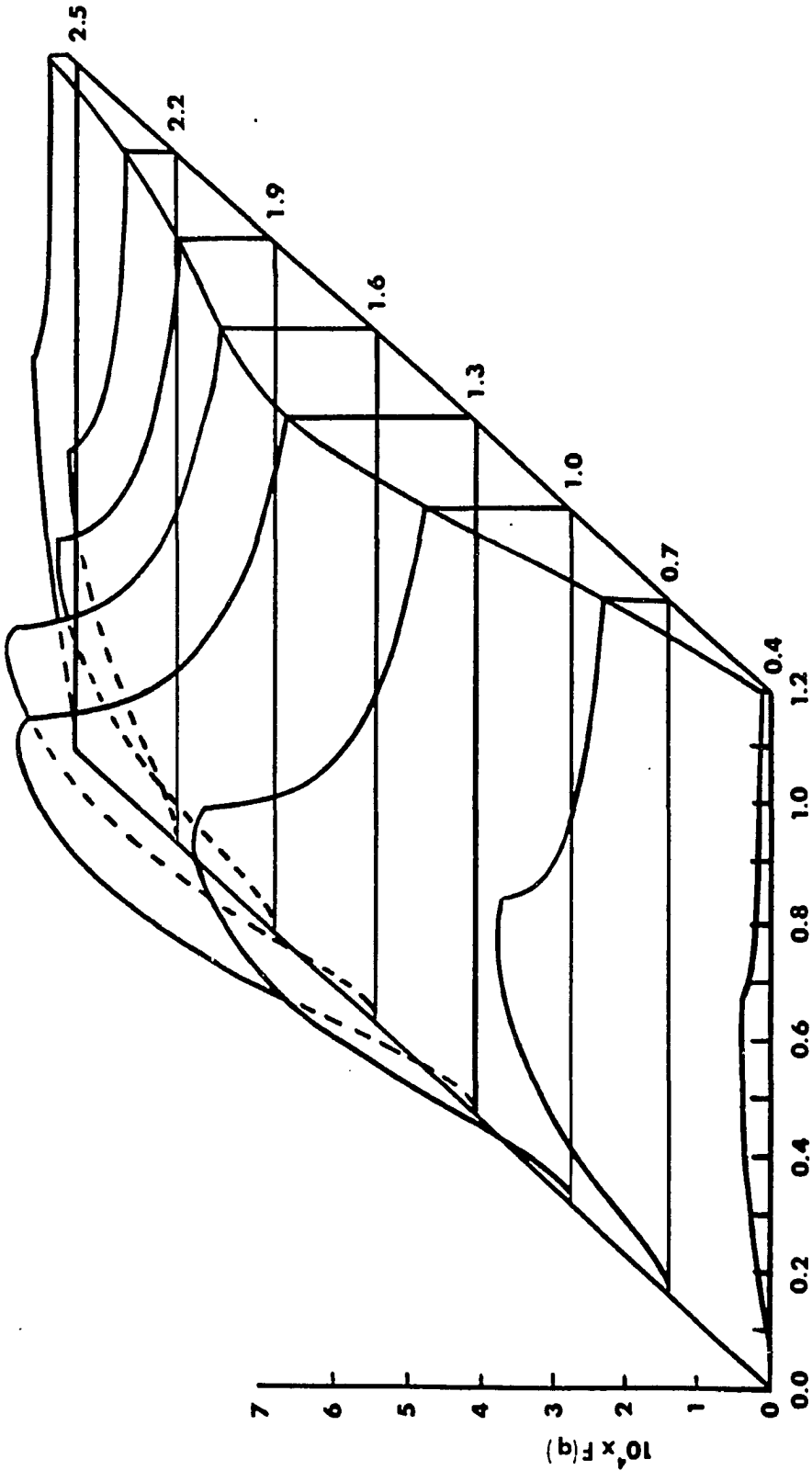

Figure 12. The Calculated RCCSM Form Factors F(q, Ep).

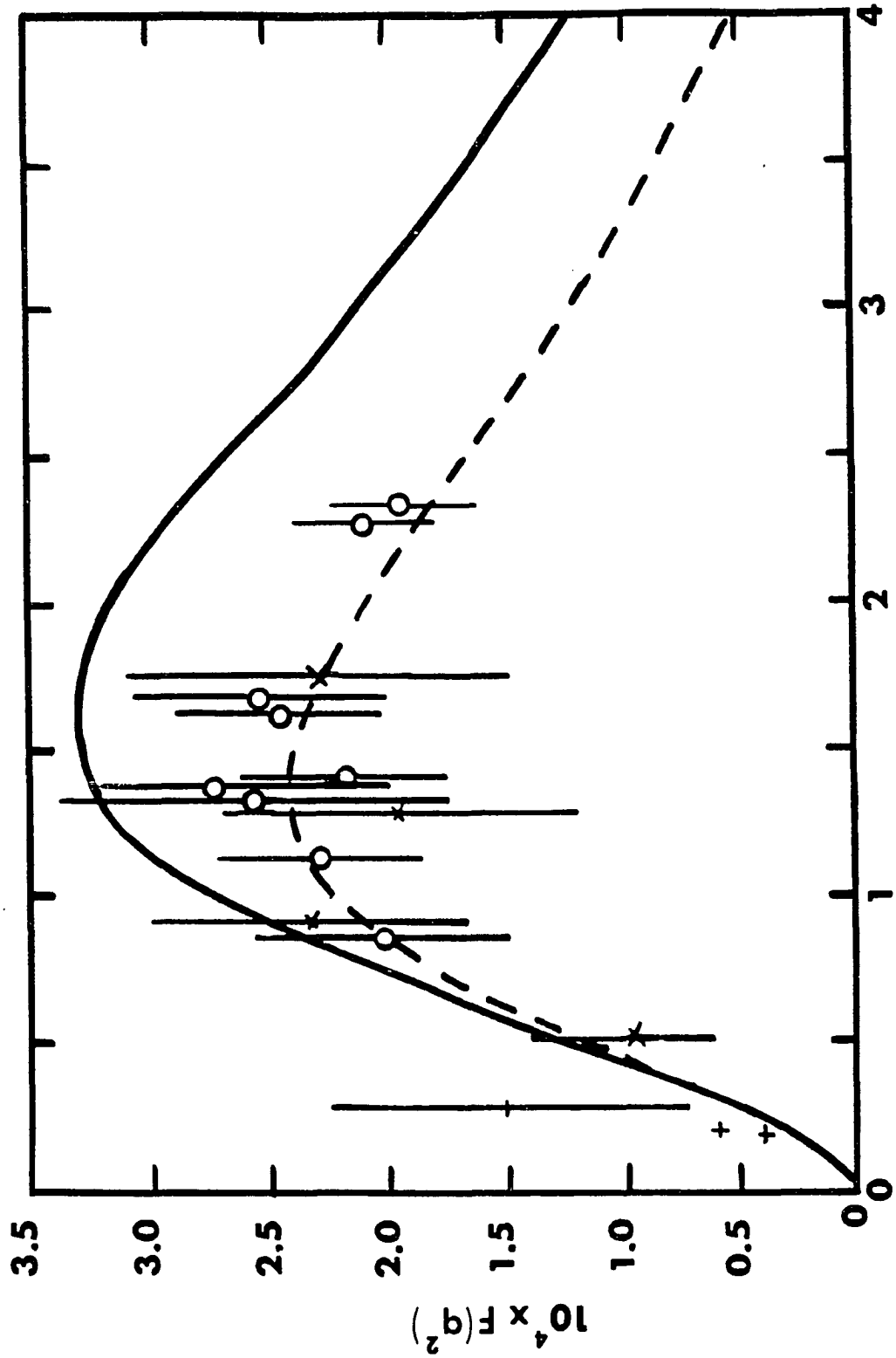

Figure 13. The Calculated RCCSM Charge Form Factors $F(q^2)$.

Curve A is the form factor with no finite proton size correction. It is obtained by integrating F(q) in figure 12 over the energy region, E_p = 0.0 – 1.1 MeV. This may include an error, since some of the 0^+ might have been assumed to be background in the experimental papers. This effect would be difficult to estimate since the different experimental papers showed different shapes and ranges for the background. The experimental form factors in figure 13, which are marked as "o", "+", and "x", are from Frosch, Rand, Yearian, Crannell & Suelzle(1965), Walcher(1970) and Kobschall et al.(1983). The original data, which are attached in appendices, are differential cross sections $d\sigma/d\Omega$, The form factors are obtained by equation (1.18). As one can see, curve A is too large and the shape is not quite correct.

If curve A is multiplied by the finite proton size correction factor,

$$1/(1 + 0.0533q^2)^4,$$

the final RCCSM 0^+ form factor (curve B) is then produced. As one can see now in figure 13, the calculated recoil corrected continuum shell model form factors, with all coordinate consideration and assuming a pure $0s^4$ ground state and discarding $0s^4$ components in the excited state, agree with experiment very well. The shape is correct, so is the strength of the form factor.

CHAPTER IV

CONCLUSION AND A SUGGESTION FOR FURTHER RESEARCH

The major task of this paper was to calculate the electro-excitation charge form factors of ^{4}He, 0^+ state within the context of the recoil corrected continuum shell model. Inelastic electron scattering experiments (Kobschall et al., 1983; Watcher, 1970; Forsch, Rand, Yearian, Crannell & Suelzle, 1965) have shown that the 0^+ state accounts for a very small percentage of the energy weighted sum rule and previous shell-model calculations, which assume a $1s0s^{-1}$ ($J = 0$, $J = 0$) configuration, over-predicted the strength by a factor of 20 (Lui & Zamick, 1986). This has led to speculations that the shell model is inappropriate for describing this light system. The present calculation, employed the recoil corrected continuum shell model with full target internal coordinate considerations, showed that the shell model does describe the ^{4}He system. The crucial ingredients of the recoil corrected continuum shell model were a realistic interaction, translationally invariant wave functions and proper boundary conditions. Also, the full center of mass correction to the form factor was taken into account.

The result was then compared with the experimental data. Excellent agreement between the calculated and experimental form factors was achieved.

However, one must remember that it is not correct to treat the ^4He ground state as a pure $0s^4$. Halderson and Philpott (Halderson & Philpott, 1979) have included $ns0s^{-1}$ correlations as a correction into the ground state wave function for the $^4He(\gamma, p)^3H$ reaction in 1979. Figure 14 shows their calculated cross section while comparing with experiment for the reaction. The

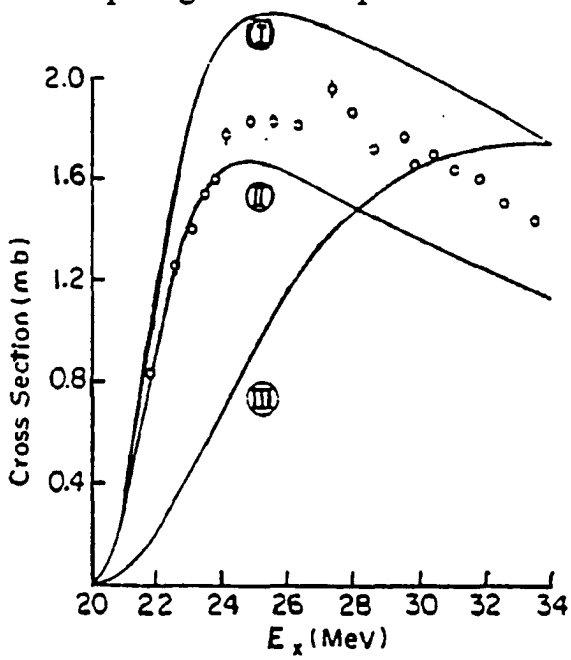

Figure 14. Cross Section For The $^4He(\gamma, p)^3H$ Reaction. Curve I is for a pure $Os_{1/2}$, ^4He ground state; curve II is an estimate of including ground state correlations; curve III is the uncorrected cross section.

ground state correlations did a good job in correcting the ground state structure here. So for future research, it is suggested that the ground state correlations $ns0s^{-1}$ should be taken into account in calculating $^4He(e, e')^4He(0^+)$ form factors.

APPENDICES A

Experimental Data From Kobschall et al., 1983

Table 1

. Differential cross sections of the quasi-bound state in ^4He

q^2 (fm^{-2})	E_o (MeV)	θ (deg)	$d\sigma/d\Omega$ ($10^{-6} fm^2/sr$)
0.843	319.95	34.28	4.96±1.42
1.124	319.95	39.89	3.05±0.62
1.332	179.94	86.70	0.39±0.13
1.368	229.94	64.63	0.93±0.27
1.405	319.95	44.96	1.74±0.40
1.641	229.94	71.98	0.51±0.11
1.687	319.95	49.65	1.35±0.33
2.220	179.94	128.29	0.07±0.04
2.279	229.94	88.59	0.17±0.04
2.342	319.95	59.70	0.46±0.07

APPENDICES B

Experimental Data From Walcher, 1970

Table 2

Results for the 20.5 MeV level of the α particle

E_0 (MeV)	θ (deg)	q^2 (fm^{-2})	$d\sigma/d\Omega$ ($10^{-33} cm^2/ster$)
198	45	0.52	22 ±5
200	60	0.90	15 ±3
198	75	1.29	4.8±1.2
200	90	1.75	2.4±0.6

APPENDICES C

Experimental Data From Frosch, Rand, Yearian, Crannell & Suelzle, 1965

Table 3

Results for the 20 MeV level of the α particle

E_0 (MeV)	θ (deg)	q^2 (fm^{-2})	$d\sigma/d\Omega$ (nb/sr)
149.3	45.0	0.286	80.6 ±38.3
149.3	86.3	0.890	12.5 ± 5.0
169.2	39.7	0.295	106 ±45
199.1	45.0	0.526	67.8 ±21.0
199.1	60.0	0.890	48.6 ±14.5
199.1	75.0	1.30	15.1 ± 5.0
199.1	90.0	1.74	7.75± 2.60
298.8	38.0	0.890	94.6 ±27.8
298.8	54.6	1.74	31.5 ± 9.3
398.4	39.7	1.74	47.0 ±13.8
398.4	45.0	2.20	30.7 ± 9.0
398.4	50.0	2.66	14.1 ± 4.1
398.4	60.0	3.67	4.90± 1.96

BIBLIOGRAPHY

Bertsch, G., Borysowicz, J., McManus, H., & Love, W. G. Interaction for inelastic scattering derived from realistic potentials. Nucl. Phys. A284(1977)399.

Blilie, C. L., Dehnhard, D., Holtkamp, D. B., Seestrom-Morris, S. J., Nanda, S. K., Cottingame, W. B., & Halderson, D. Measurement of Isospin Mixing in ^{4}He and Its Implications for Charge-symmetry Breaking. Phys. Rev. Lett. 57B(1986)543.

Crone, L., & Werntz, C. Electron and Proton Excitation of ^{4}He continuum states. Bull. Am. Phys. Soc. 12(1967)12.

DeForest, T., & Walecka, J. D. Electron scattering and nuclear structure. Adv. Phys. 15(1966)1.

Fano, U. Effects of Configuration Interaction on Intensities and Phase Shifts. Phys. Rev. 124(1961)1866.

Fiarman, S., & Meyerhoff, W. E. Energy levels of light nuclei A = 4. Nucl. Phys. A206(1973)1.

Flowers, B. H. The nuclear shell model. Prog. Nucl. Phys. 2(1952) 235.

Frosch, R., Rand, R. E., Yearian, M. R., Crannell, H. L., & Suelzle, L. R. Inelastic electron scattering from the ALPHA particle. Phys. Lett. 19(1965)155.

Furutani, H., Horiuchi, H., & Tamagaki, R. Strcture of the second 0^+ state of ^{4}He. Prog. Theor. Phys.60(1978)307.

Halderson, D., & Philpott, R. J. Recoil corrected continuum shell model calculations for four-nucleon systems. Nucl. Phys. A321(1979)295.

Halderson, D., Philpott, R. J., Carr, J. A., & Petrovich, F. Pion inelastic scattering to particle unbound stretched states of ^{12}C. Phys.Rev. C24(1981)1095.

Kobschall, G., Ottermann, C., Maurer, K., Rohrich, K., Schmitt, Ch., & Walther, V. H. Excitation of the quasi-bound state in ^{4}He by electron scattering at medium momentum transfer. Nucl. Phys. A405(1983)648.

Lane, A. M., & Tomas, R. G. R-matrix theory of nucear reactions. Mod. Phys. 30(1958)257.

Lane, A. M., & Robson, D. Comprehensive formalism for nuclear reaction problems. Rev. Phys. Rev. 151(1966)774.

Lui, H., & Zamick, L. Amount of breathing mode admixture in the first excited state of ^{4}He. Phys. Rev. C35(1986)445.

Mahaux, C., & Weidenmuller, H. A. Shell model approach to nuclear reactions (North-Holland, Amsterdam, 1969).

Philpott, R. J., & George, J. On the practical application of the generalized R-matrix method to problems in nuclear. Nucl. Phys. A233(1974)164.

Philpott, R. J. Continuum shell model with full corrction for target recoil. Nucl. Phys. A289(1977)109.

Samyal, S., & Mukherjee, S. N. Inelastic electron scattering charge form factor of ^{4}He. Phys. Rev. C36(1987)67.

Watcher, T. Excitation of ^{4}He by inelastic electron scattering at low momentum transfer. Phys. Lett. 31B(1970)442.